JOURNAL OF SOLID STATE CHEMISTRY 109, 47–52 (1994)

# $Li_{1-x-y}H_yCoO_2$: Metastable Layered Phases Obtained by Acid Digestion of $LiCoO_2$(O3)

E. Zhecheva and R. Stoyanova

*Institute of General and Inorganic Chemistry, Bulgarian Academy of Sciences, 1113 Sofia, Bulgaria*

Received August 5, 1992; in revised form March 12, 1993; accepted June 18, 1993

Metastable layered phases of lithium-containing cobalt oxyhydroxides $Li_{1-x-y}H_yCoO_2$($x \leq 0.55$, $x + y < 1$) are obtained by acid digestion of $LiCoO_2$ at room temperature. X-ray powder diffraction, thermal analysis, magnetic susceptibility measurements, and EPR are used to investigate the structural peculiarities of these phases. It has been shown that the layered $CoO_2$ framework of parent $LiCoO_2$ is retained during acid treatment. Lithium extraction from the $LiO_2$ layers introduces $Co^{4+}$ ions in the $CoO_2$ layers, which, with progressive lithium removal, tend to segregate as demonstrated by EPR and magnetic susceptibility measurements. In addition, lithium extraction enters into competition with exchange of lithium ions with protons, depending on the acid concentration and on the dissolution degree of the samples. The simultaneous presence of $Li^+$ and $H^+$ in the $CoO_2$ matrix, as well as the $Co^{4+}$ clustering, provokes a certain disorder in the parent layered structure and determines the thermal instability of acid-treated $LiCoO_2$. On heating, cation redistribution is initiated in the metastable phases, culminating above 230°C in thermal decomposition into a lithium–cobalt spinel. 

## INTRODUCTION

Soft chemistry reactions (intercalation, deintercalation, ion exchange, etc.) provide new perspectives on materials design (1). In recent years, scientific efforts have been focused on lithium–nickel and lithium–cobalt oxides, $LiMO_2$ ($M$ = Co and Ni) (2), which are of interest for lithium batteries (3). For example, a new crystal modification of the well-known $LiCoO_2$ (designated as $LiCoO_2$(O2)) has been synthesized by ion exchange between $Na^+$ from $Na_{1-x}CoO_2$(O2) and $Li^+$ from a LiCl methanol solution (4). Both crystal modification of $LiCoO_2$ (O3 and O2) display different delithiation properties: the lithium extractions from $LiCoO_2$(O3) yield a single $Li_{1-x}CoO_2$($x \leq 0.67$) phase inheriting the structural framework of parent $LiCoO_2$ (5, 6), while the crystal structure of $LiCoO_2$(O2) changes during the lithium removal (7). Well-crystallized $\gamma$-type cobalt-substituted nickel oxyhydroxides (P3) with a mean oxidation state of (Ni + Co) of about 3.5 are obtained by hydrolysis of $NaCo_xNi_{1-x}O_2$ ($x \leq 0.5$, (O3)) in an alkaline medium (8–10). The formation of $\gamma$-type oxyhydroxides in an alkaline medium is closely related to the insertion of alkali ions ($K^+$ and/or $Na^+$) and water from the mother solution in the interlayer space of the crystal lattice, i.e., $Na_x(H_3O)_yNiO_2$ or $K_x(H_3O)_yNiO_2$. In strong acids (pH $\leq$ 2), these authors (10) found complete conversion of $NaCo_xNi_{1-x}O_2$ ($x \leq$ 0.5, O3) to the stable modification of the oxyhydroxide $\beta$-$Ni_{1-x}Co_xOOH$ (O1). As far as we know, there are no data on the formation of cobalt analogies of $\gamma$-type oxyhydroxides containing alkali ions in the space between the $CoO_2$ layers and having an oxidation state of Co above 3. The investigations of Tirado and co-workers (11, 12) have shown that hydrolysis of $Co(NH_3)_6^{3+}$ in a concentrated LiOH solution (11) and hydrothermal treatment of $LiCoO_2$(O3) at 200°C in HCl (12) lead to a fine mixture of CoOOH (P3) and $LiCoO_2$(O3) but not to a lithium-containing cobalt oxyhydroxide. On the other hand, in previous studies we have shown that the thermal decomposition of CoOOH in a $LiNO_3$ melt is preceded by partial exchange between the protons from CoOOH and $Li^+$ from the melt (13). We have not succeeded in isolating this "hypothetical" lithium–cobalt oxyhydroxide phase ($Li_{1-x}H_xCoO_2$) because under the conditions of its formation it is decomposed to a lithium–cobalt spinel. Taking into account the above results, we have tried to prepare a lithium-containing cobalt oxyhydroxide by acid treatment of $LiCoO_2$(O3) at room temperature.

## EXPERIMENTAL

The initial salts used for the preparation of $LiCoO_2$ were $Li_2CO_3$ and $Co(NO_3)_2 \cdot 6H_2O$ (Li : Co = 1.05). Lithium carbonate was added to a solution of $Co(NO_3)_2$ (75 wt%) and the mixture was evaporated, heated at 220°C until the nitrogen oxides evolved completely, then ground and heated at 500°C for 6 hr. The mixture was ground again, pelleted, and heated at 750°C for 36 hr.

To achieve $LiCoO_2$ hydrolysis, 2 g of the samples were



0022-4596/94 $6.00

treated at room temperature with 100 ml of 0.1, 1, and 8 $N$ $H_2SO_4$ for 24, 2, and ½ hr, respectively. For the sake of comparison, 1 $N$ HCl was also used for acid treatment. The different durations of acid treatment were chosen so as to ensure dissolution of about 50–70% of the initial $LiCoO_2$ samples. The solid residues thus obtained were rinsed with water and dried at room temperature. For the sake of convenience, the acid-treated samples are denoted hereafter by $LiCoO_2$–A.

The lithium content was determined by atomic absorption analysis. The total cobalt content was established by complexometric titration, and the mean oxidation state of Co was determined by iodometric titration.

The phase composition of the samples was checked by X-ray powder diffraction (XRD) using a Philips diffractometer with Cu$K\alpha$- radiation. The specific surface area of the samples was determined by the BET method.

DTA and TG measurements were carried out with a Stanton Redcroft (England) apparatus in platinum crucibles with a diameter of 5 mm at temperatures of 20–1000°C and a heating rate of 10°/min.

The magnetic susceptibility was determined by the Faraday method at 100–600 K. The EPR spectra were recorded with a Bruker ERS-300 spectrometer within the temperature range of 4.2–300 K.

## RESULTS AND DISCUSSION

The chemical compositions of the acid-treated samples are summarized in Table 1. Obviously, the lithium amount strongly decreases with rising acid concentration, as well as with increasing dissolution degree of the samples. However, we have not succeeded in complete extraction of the $Li^+$ ions from $LiCoO_2$ by chemical delithiation: the minimum amount of Li that remains in the delithized samples is Li/Co ≅ 0.04. The mean oxidation state of Co (OS) is higher than 3 (Table 1) after acid digestion of all the samples studied, but, to the Li amount, OS does not change monotonically with acid concentration: the highest oxidation state (3.5) is found with samples treated with 1 $N$ $H_2SO_4$ (Table 1). Besides, the chemical composition of $LiCoO_2$–A does not depend on whether $H_2SO_4$ or HCl was used. The discrepancy between the changes in lithium amount and OS after acid digestion (Table 1) is an unexpected result, but this result implies that the acid can act toward $LiCoO_2$ both as a delithizing and a hydrolyzing agent.

Despite the drastic change in chemical composition of the acid-treated samples, the X-ray diffraction patterns of $LiCoO_2$–A are similar (in terms of line positions) to that of initial $LiCoO_2$, which is indexed to the trigonal

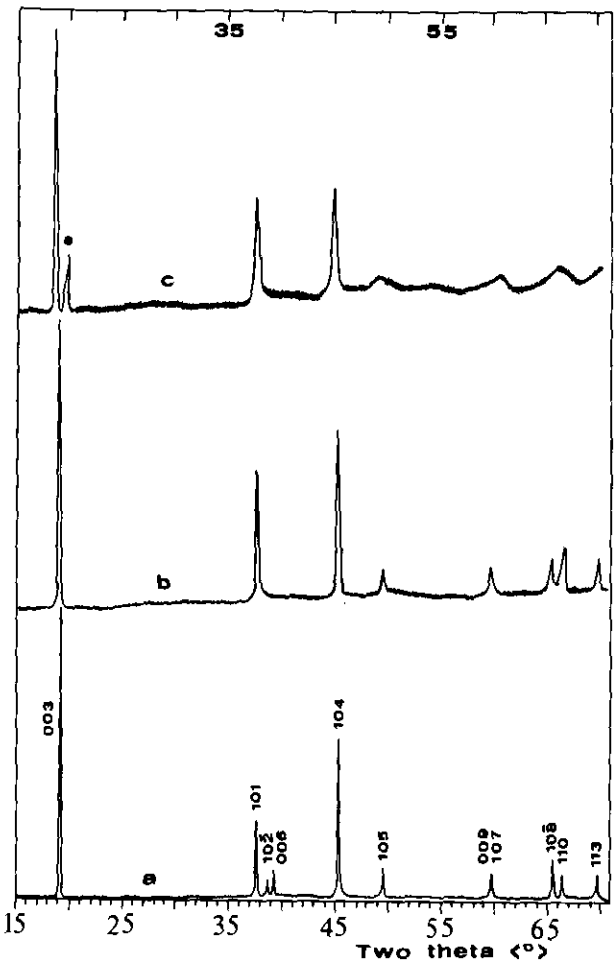


FIG. 1. X-ray patterns of $LiCoO_2$ (a), $LiCoO_2$ treated with 0.1 $N$ $H_2SO_4$ (b) and $LiCoO_2$ treated with 1 $N$ $H_2SO_4$ to a dissolution degree of 70% (c). The Miller indices of the Bragg peaks are indicated near each line. The circles denote the line with $d$ = 4.50 Å not belonging to the initial XRD patterns.

TABLE 1

**Lithium Content (wt%) and Mean Oxidation State (OS) of Cobalt Ions of the Acid-Treated $LiCoO_2$ Samples until Corresponding Dissolution Degree (DD)**

| Acid | DD (%) | Li (wt%) | OS | $Li^+_{1-x-y}$ | $H^+_y$ | $Co^{3+}_{1-x}$ | $Co^{4+}_x$ |
|---|---|---|---|---|---|---|---|
| 0.1 $N$ $H_2SO_4$ | 45 | 5.14 | 3.15 | 0.71 | 0.14 | 0.85 | 0.15 |
| 1 $N$ $H_2SO_4$ | 50 | 2.65 | 3.42 | 0.36 | 0.22 | 0.58 | 0.42 |
| 8 $N$ $H_2SO_4$ | 50 | 0.58 | 3.16 | 0.08 | 0.76 | 0.84 | 0.16 |
| 1 $N$ HCl | 55 | 2.40 | 3.51 | 0.32 | 0.17 | 0.49 | 0.51 |
| 8 $N$ $H_2SO_4$ | 65 | 0.30 | 3.36 | 0.04 | 0.60 | 0.64 | 0.36 |
| 1 $N$ $H_2SO_4$ | 70 | 1.00 | 3.53 | 0.13 | 0.34 | 0.47 | 0.53 |
| $LiCoO_2$ | — | 7.10 | 2.99 | 1.0 | — | 1.0 | — |

*Note.* Chemical composition of $LiCoO_2$–A calculated according to the chemical formula $Li^+_{1-x-y}H^+_y\,Co^{3+}_{1-x}\,Co^{4+}_x\,O_2$.

space group $R\bar{3}m$ (Fig. 1). Only the XRD pattern of the sample with the highest Co oxidation state (3.59) exhibits an additional weak asymmetric diffraction peak with $d$ = 4.50 Å (Fig. 2). It is interesting to note that only this peak ($d$ = 4.50 Å) is observed in the XRD pattern of $LiCoO_2$ completely delithiated to $CoO_2$ by powerful chemical oxidants in a nonaqueous medium (6). Since the X-ray scattering factor of lithium is smaller than those of cobalt and oxygen, the similarity of the X-ray patterns of $LiCoO_2$–A and $LiCoO_2$ indicates clearly that the structural framework of parent $LiCoO_2$ is retained during acid dissolution. As is well known, the structural framework of $LiCoO_2$ can be described as a close-face-centered-cubic packing of oxygen ions, where the octahedral sites are alternatively occupied by $Li^+$ and $Co^{3+}$, making up $LiO_2$ and $CoO_2$ layers ($\alpha$-$NaFeO_2$ type crystal structure) (14). The acid digestion of $LiCoO_2$ is manifested by a broadening of the XRD lines (Fig. 2a) and by a "grinding" of the samples (as illustrated by the increase of the specific surface area, Fig. 2b). Thus, the line broadening can be attributed to a reduction of crystallinity during acid treatment of $LiCoO_2$. It is important to emphasize that, for acid-treated samples, the widths of the XRD peaks increase noticeably with increasing scattering angle (Fig. 2a). This means that, in addition to particle size effects, strains (resulting from stacking disorder, turbostratic effects, cation clustering, etc.) also contribute to the XRD line width. The structural disorder in layered $LiCoO_2$–A may explain the slight variations in the relative intensities of the diffraction peaks (003), (101), and (104) (Fig. 3a). Furthermore, the acid digestion of $LiCoO_2$ results in an expansion of the $d_{003}$ spacing, which corresponds to the interlayer spacing in the hexagonal $\alpha$-$NaFeO_2$ type structure (Fig. 3b). The expansion of the interlayer spacing (Fig. 3b) with lithium extraction was also observed for electrochemically delithiated $LiCoO_2$ and was explained by the electrostatic repulsions between lithium-depleted layers (5, 7, 15). From the X-ray and chemical analysis data, we can conclude that acid digestion of $LiCoO_2$ proceeds simultaneously with lithium extraction and proton exchange in the framework of the parent layered structure. In other words, it appears that a layered lithium containing cobalt oxyhydroxide is formed during partial dissolution of $LiCoO_2$:

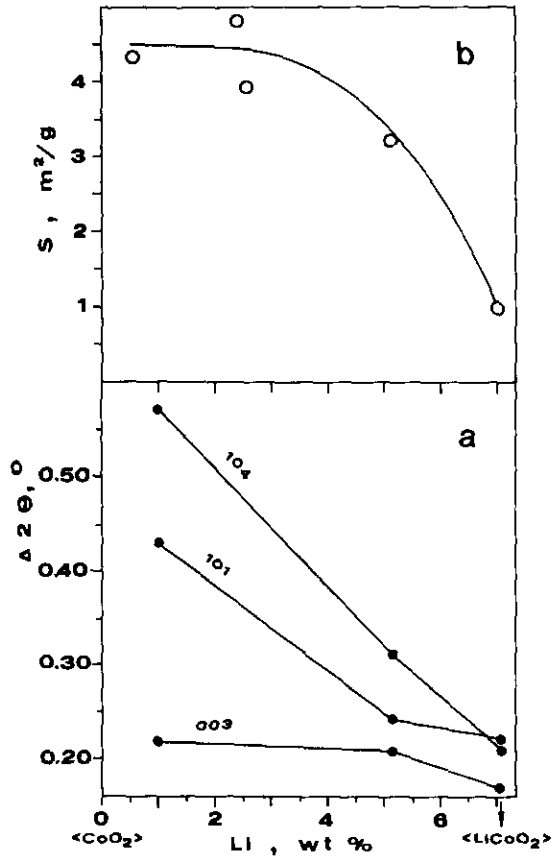


FIG. 2. (a) XRD line widths at half maximum intensity of (003), (101), and (104) versus lithium content. (b) Specific surface area of $LiCoO_2$–A versus lithium content.

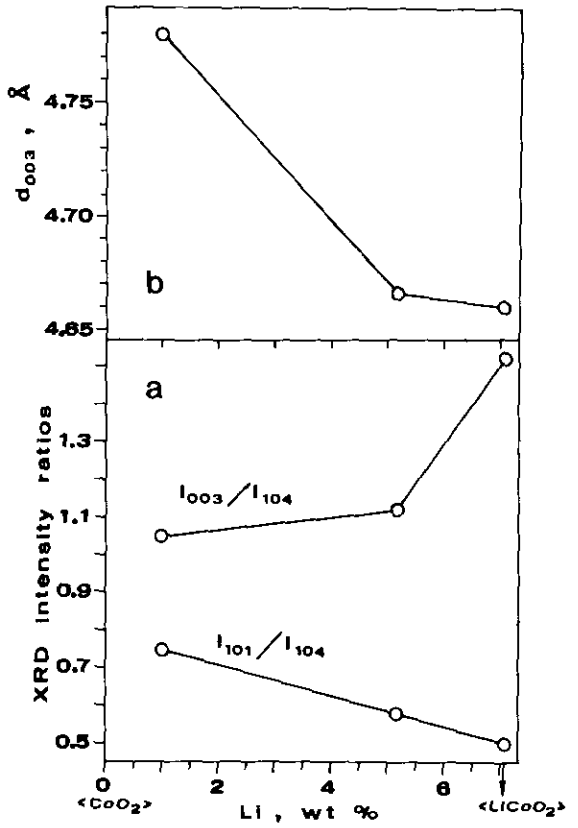


FIG. 3. (a) XRD intensity ratios of $I_{003}/I_{104}$ and $I_{101}/I_{104}$ versus lithium content. (b) Dependence of $d_{003}$ spacing on the lithium content.

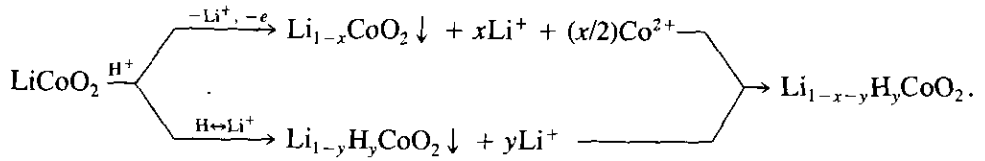


DTA and TG data give further information on the proton content in acid-delithiated $LiCoO_2$. The thermochemical behaviors of $LiCoO_2$–A are compared to that of CoOOH in Fig. 4. According to Refs. (12, 13), CoOOH dehydrates endothermally into the spinel $Co_3O_4$ at 280–360°C, which is further decomposed to CoO with a rock-salt structure at 910–940°C. In the thermochemical behavior of acid-treated $LiCoO_2$, two temperature regions can also be distinguished: decomposition between 200 and 500°C to a spinel (as evident by XRD data) and further decomposition of this spinel between 840 and 920°C. In the low-temperature region, the DTA curves of $LiCoO_2$–A display two irreversible thermal effects: an exo effect at 150–230°C and an endo effect at 230–290°C (Fig. 4a). The weight loss of $LiCoO_2$–A (Fig. 4b) does not begin below 200°C; between 230 and 300°C, the main weight loss is observed; and, with further heating up to 500°C, the decomposition process is slowed down. The decomposition product of $LiCoO_2$–A is a lithium-containing spinel, which is evidenced by the lower temperature of the "spinel–rock salt" transition as compared to that of pure $Co_3O_4$ (850°C compared to 920°C, respectively, Fig. 4), as was shown in Ref. (17). Using the data from the chemical analysis of $LiCoO_2$–A (Table 1) one can calculate the weight loss during the endothermal decomposition of the acid-treated $LiCoO_2$ to a lithium–cobalt spinel. Table 2 presents the experimental weight loss of $LiCoO_2$–A at 200–500°C as well as the calculated weight loss according to reaction scheme 1, comprising a lithium–cobalt spinel as the decomposition product. As one can see, the calculated weight loss for the samples with a high lithium content is much lower than the experimental weight loss, suggesting some problems with the proposed reaction scheme of decomposition of $LiCoO_2$–A to lithium–cobalt spinel. According to this reaction scheme, the calculated lithium amount in the cobalt spinel is above 12 at.% (Table 2), which contradicts our previous data (13, 17) on the maximal lithium content in a lithium–cobalt spinel obtained at 500°C (up to 12 at.%). To overcome this problem, Table 2 presents the calculated weight loss for an extreme case, where $LiCoO_2$–A transforms to $LiCoO_2$ and $Co_3O_4$ (reaction scheme 2). The comparison between calculated and experimental weight loss indicates that the decomposition of the acid-treated samples, $Li_{1-x-y}H_yCoO_2$, proceeds to cobalt spinel with a lower lithium content and $LiCoO_2$. The weak exothermic effect between 190 and 230°C (Fig. 4a), which is not associated with any weight loss, can be explained by a structural variation of $Li_{1-x-y}H_yCoO_2$. Due to the overlapping of the exo and endo effects (Fig. 4a), an exact interpretation of the exo effect is difficult. Thus, DTA and TG data reveal the simultaneous presence of both $H^+$ and $Li^+$ in the structure of acid-treated $LiCoO_2$–A.

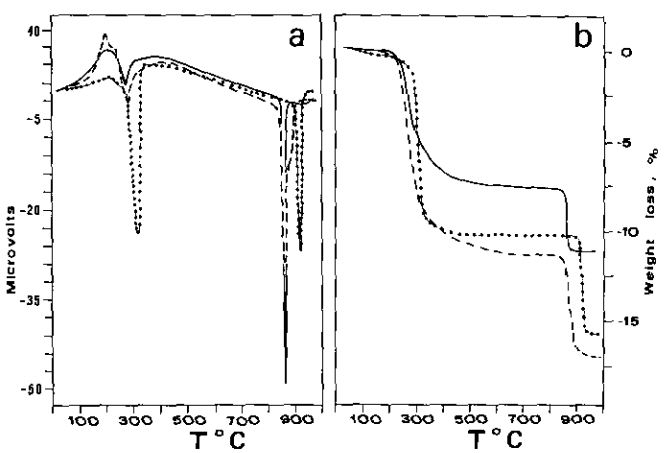


FIG. 4. DTA (a) and TG (b) profiles of CoOOH (dotted curves), $LiCoO_2$ treated with 1 $N$ $H_2SO_4$ to a dissolution degree of 50% (dashed curves), and $LiCoO_2$ treated with 8 $N$ $H_2SO_4$ to a dissolution degree of 50% (full curves).

Having in mind the different magnetochemical properties of low-spin $Co^{3+}$ and $Co^{4+}$ ions ($S = 0$ and $S = \frac{1}{2}$, respectively), EPR and magnetic susceptibility measurements were used to prove the charge compensation in acid-treated $Li_{1-x}H_xCoO_2$ samples. The EPR spectrum of the sample treated with 0.1 $N$ $H_2SO_4$ consists of an axially anisotropic signal with $2.40 \leq g_\perp \leq 2.49$ and $g_\parallel \cong 1.89$ at 4.2 K (Fig. 5), which saturates with increasing microwave power and registration temperature. These parameters of the EPR signal are assigned to the low-spin $Co^{4+}$ ions with a triplet ground state ($^2T_{2g}$) and occupying an axially distorted octahedral crystal field. The registration of $Co^{4+}$ by EPR is the first direct experimental proof for the presence of $Co^{4+}$ in the $CoO_2$ slabs, caused by lithium extraction from $LiCoO_2$. For the $LiCoO_2$–A samples with a lower lithium content (Table 1), an EPR signal of $Co^{4+}$ is not observed, which may be explained by the clustering of $Co^{4+}$ and/or the loss of crystallinity. In an attempt to investigate the $Co^{4+}$ distribution in the $CoO_2$ slabs, Fig. 6 presents the temperature variation of the magnetic susceptibility ($\chi$) of $LiCoO_2$–A, as compared with CoOOH, in coordinates $1/\chi$ vs $T$. The small values of $\chi$

TABLE 2

**Experimental Weight Loss of Acid-Treated Samples at 200–500°C, Calculated Weight Loss According to Reaction Schemes (1) and (2), and Calculated Lithium Amount ($a$) in the Lithium–Cobalt Spinel ($Li_aCo_{3-a}O_4$) Formed According to Scheme (1)**

| Samples (DD, %) | Weight loss (%) $200 < T < 500$ | Weight loss (%) according to schemes (1) | (2) | $a$, $Li_aCo_{3-a}O_4$ according to scheme (1) |
|---|---|---|---|---|
| 1 $N$ $H_2SO_4$ (50) | 7.01 | 3.47 | 7.55 | 0.54 |
| 1 $N$ HCl (55) | 7.53 | 4.25 | 7.93 | 0.44 |
| 8 $N$ $H_2SO_4$ (50) | 10.96 | 10.61 | 11.51 | 0.22 |

$$Li_{1-x-y}H_yCoO_2 \downarrow$$

$$(2-x-y)/3\ Li_{3(1-x-y)/(2-x-y)}Co_{3/(2-x-y)}O_4 + y/2\ H_2O + (4x+5/2y-2)/6\ O_2. \quad (1)$$

$$(1-x-y)\ LiCoO_2 + (x+y)/3\ Co_3O_4 + y/2\ H_2O + (4x-6)/12\ O_2. \quad (2)$$

of the diamagnetic CoOOH below 470 K are due to the temperature-independent paramagnetism of low-spin $Co^{3+}$ ($S = 0$) and $Co^{2+}$ impurity ions. Above this temperature, the diamagnetic CoOOH is decomposed to the paramagnetic $Co_3O_4$ ($T_N \cong 40$ K) (16), which is visualized by a sharp increase of $\chi$ in the heating curve. The cooling curve corresponds to the temperature dependence of $\chi$ of $Co_3O_4$ thus obtained. The comparison of the magnetic behavior of CoOOH and acid-treated samples (Fig. 6) reveals the following features:

(i) at room temperature, $\chi$ of all $LiCoO_2$–A studied is higher than $\chi$ of CoOOH due to the presence of low-spin $Co^{4+}$ ions ($S = \frac{1}{2}$);

(ii) regardless of the composition, between 100 and 300 K the variations in $\chi$ of $LiCoO_2$–A are reversible and do not obey the Curie–Weiss law;

(iii) above 300 K, $\chi$ of the $LiCoO_2$–A samples changes irreversibly;

(iv) the sharp increase in $\chi$ for $LiCoO_2$–A corresponds to the thermal decomposition of acid-treated samples into lithium–cobalt spinels;

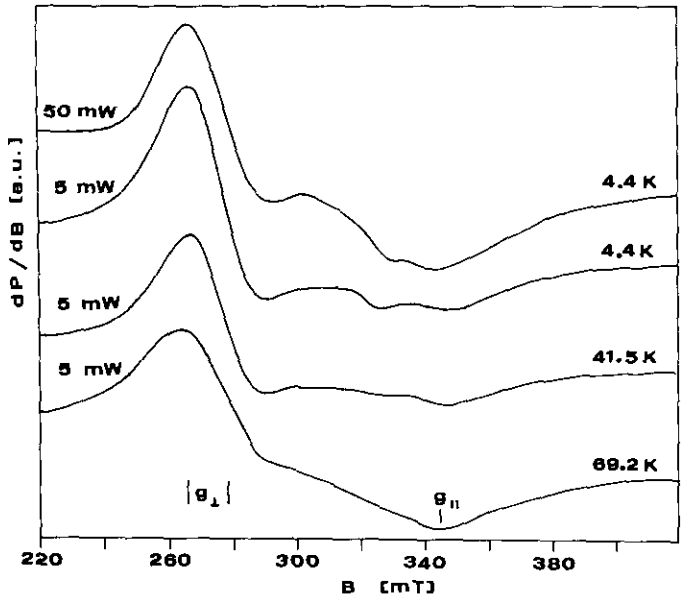


FIG. 5. Temperature variation and microwave power dependence of the EPR spectrum of $LiCoO_2$ treated with 0.1 $N$ $H_2SO_4$.

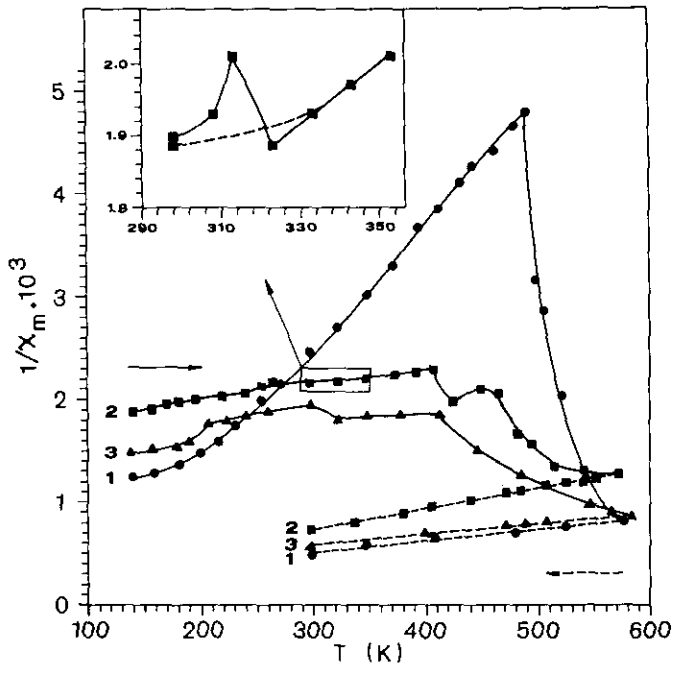


FIG. 6. Temperature variation of magnetic susceptibilities of CoOOH (●), $LiCoO_2$ treated with 1 $N$ $H_2SO_4$ to a dissolution degree of 50% (■), and $LiCoO_2$ treated with 8 $N$ $H_2SO_4$ to a dissolution degree of 50% (▲). Full curve and dashed curve in each case represent the heating curve and the cooling curve, respectively.

(v) the cooling curves correspond to the magnetic susceptibilities of the lithium–cobalt spinel oxides, the $\chi$-values depending on the lithium content.

Feature (ii) shows, once more, that the $Co^{4+}$ ions segregate in the $CoO_2$ slabs during acid treatment of $LiCoO_2$. The irreversible changes in $\chi$ for $LiCoO_2$–A below its thermal decomposition temperature reveal some structural modifications in acid-treated $LiCoO_2$ samples, which are also visible in the DTA curves (the exothermic peak at 180–230°C, Fig. 4a). This result may explain the data of Thackeray and co-workers (18) on a cation redistribution which occurs during acid delithiation of $LiCoO_2$ obtained at low temperature (400°C): the acid-treated samples of Thackeray and co-workers (18) have been dried at 80°C for 48 hr. Summarizing, layered $Li_{1-x-y}H_yCoO_2$, obtained at room temperature by acid digestion of layered $LiCoO_2$, are metastable phases; on heating above room temperature, cation redistribution is initiated, which culminates above 230°C in thermal decomposition into lithium–cobalt spinels.

## CONCLUSIONS

The effect of acid treatment on alkali metal–transition metal oxides may be classified as alkali ion extraction or proton exchange. Usually, the parent crystal structure is preserved during alkali ion extraction ($LiMn_2O_4 \rightarrow \lambda$-$MnO_2$, Ref. 19), while alkali ions exchange with protons produces structural varieties of the initial crystal structure ($NaNi_{1-x}Co_xO_2 \rightarrow \beta$-$Ni_{1-x}Co_xOOH$, Refs. 8–10). Our results indicate that the acid acts toward the layered $LiCoO_2$ (space group $R\bar{3}m$, O3) not only as a delithizing agent but also as a hydrolyzing agent, and a metastable $Li_{1-x-y}H_yCoO_2$ phase with a layered structure is formed. The chemical composition of $Li_{1-x-y}H_yCoO_2$ is specified by a competition between lithium extraction and proton exchange, depending on the acid concentration and on the degree of sample dissolution. These two competitive reactions proceed without destruction of the structural $CoO_2$ framework of parent $LiCoO_2$ (Fig. 1). The simultaneous presence of lithium ions and protons in the $CoO_2$ matrix, as well as $Co^{4+}$ segregation (as evident from magnetic data, Figs. 5 and 6), provokes structural disorder (Figs. 2 and 3) and results in thermal instability of the layered structure (Fig. 4).

## ACKNOWLEDGMENTS

The authors thank Prof. D. Reinen (Philipps Universität, Marburg, Germany) for helpful discussions, Mr. S. Hristov for DTA and TG measurements, and the Bulgarian Ministry of Education and Sciences for financial support (Contract Ch-83/1991).

## REFERENCES

1. C. Delmas, *in* "Chemical Physics of Intercalation" (A. P. Legrand and S. Frandrois, Eds.), p. 209. Plenum, New York, 1988.
2. J. B. Goodenough, *in* "31st International Congress of Pure and Applied Chemistry," p. 120, Section 5 (1987).
3. R. S. McMillan and E. E. Andrukaitis, *Proc.—Electrochem. Soc.* **91-3,** 416 (1991).
4. C. Delmas, J.-J. Braconnier, and P. Hagenmuler, *Mater. Res. Bull.* **17,** 117 (1982).
5. K. Mizushima, P. C. Jones, P. J. Wiseman, and J. B. Goodenough, *Mater. Res. Bull.* **15,** 783 (1980).
6. A. R. Wizansky, P. E. Rauch, and F. J. Disalvo, *J. Solid State Chem.* **81,** 203 (1989).
7. A. Mendiboure, C. Delmas, and P. Hagenmuller, *Mater. Res. Bull.* **19,** 1383 (1984).
8. C. Delmas, J. J. Braconnier, Y. Borthomieu, and P. Hagenmuller, *Mater. Res. Bull.* **22,** 741 (1987).
9. C. Delmas, J. J. Braconnier, Y. Borthomieu, and M. Figlarz, *Solid State Ionics* **28–30,** 1132 (1988).
10. C. Delmas, Y. Borthomieu, C. Faure, A. Delahaye, and M. Figlarz, *Solid State Ionics* **32–33,** 104 (1989).
11. C. Barriga, A. Calero, J. Morales, and J. L. Tirado, *React. Solids* **7,** 263 (1989).
12. J. M. Fernandez-Rodriguez, L. Hernan, J. Morales, and J. L. Tirado, *Mater. Res. Bull.* **23,** 899 (1988).
13. E. Zhecheva and R. Stoyanova, *Mater. Res. Bull.* **26,** 1315 (1991).
14. H. J. Orman and P. J. Wiseman, *Acta Crystallogr., Sect. C* **40,** 12 (1984).
15. A. Hoders, J. M. der Kinderen, A. H. van Heerden, J. H. W. de Wit, and G. J. H. Broers, *Solid State Ionics* **14,** 205 (1984).
16. W. L. Roth, *J. Phys. Chem. Solids* **25,** 1 (1962).
17. E. Zhecheva, R. Stoyanova, and S. Angelov, *Mater. Chem. Phys.* **25,** 361 (1990).
18. R. J. Gummow, M. M. Thackeray, W. I. F. David, and S. Hull, *Mater. Res. Bull.* **27,** 327 (1992).
19. J. C. Hunter, *J. Solid State Chem.* **39,** 142 (1981).